

**The walentaite group and the description of a new member, alcantarillaite, from the
Alcantarilla mine, Belalcazar, Cordoba, Andalusia, Spain**

Ian E. Grey¹, Rupert Hochleitner², Christian Rewitzer³, Alan Riboldi-Tunncliffe⁴, Anthony R. Kampf⁵, Colin M. MacRae¹, W. Gus Mumme¹, Melanie Kaliwoda², Henrik Friis⁶ and Carlos U. Martin⁷.

¹CSIRO Mineral Resources, Private Bag 10, Clayton South, Victoria 3169, Australia.

²Mineralogical State Collection (SNSB), Theresienstrasse 41, 80333, München, Germany.

³Stadtplatz 17, 93437 Furth im Wald, Germany.

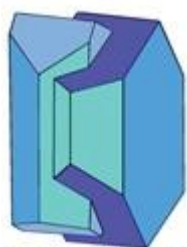
⁴Australian Synchrotron, 800 Blackburn Road, Clayton, Victoria 3168, Australia.

⁵Mineral Sciences Department, Natural History Museum of Los Angeles County, 900 Exposition Boulevard, Los Angeles, CA90007, USA.

⁶Natural History Museum, University of Oslo, PO Box 1172, Blindern, 0318 Oslo, Norway.

⁷C/ Orquidea 23, 29190, Malaga.

E-mail: ian.grey@csiro.au



Mineralogical Society

This is a 'preproof' accepted article for Mineralogical Magazine. This version may be subject to change during the production process.

DOI: 10.1180/mgm.2020.18

Abstract

The general structural formula for the walentaite group is

$[(A1_y A1'_{1-y}), A2](H_2O)_n [B_x (As2)_{2-x} (As3) M1 (M2)_2 (TO_4)_2 (O, OH)_7]$, based on heteropolyhedral layers of configuration $[M1 (M2)_2 (TO_4)_2 (O, OH)_6]$, with surface-coordinated species at the *B*, *As2* and *As3* sites, and with interlayer hydrated cation groups centred at the *A* sites. The group is divided into walentaite and halilsarpite subgroups based on $T = P^{5+}$ and As^{5+} , respectively. Alcantarillaite, (IMA2019-072), $[Fe^{3+}_{0.5} \square_{0.5} (H_2O)_4] [CaAs^{3+}_2 (Fe^{3+}_{2.5} W^{6+}_{0.5}) (AsO_4)_2 O_7]$, is a new member of the walentaite group from the Alcantarilla wolframite mine, Belalcazar, Cordoba, Andalusia, Spain. It occurs most commonly as lemon-yellow fillings together with massive scorodite in fissures and cracks in quartz adjacent to löllingite. It is also found as tiny yellow rosettes lining vugs and as spheroids of ultrathin blades. It is associated with scorodite, pharmacosiderite, ferberite and schneiderhöhnite. Optically it is biaxial (-), with $\alpha = 1.703(\text{calc})$, $\beta = 1.800(5)$, $\gamma = 1.850(5)$, $2V = 68(1)^\circ$ (white light). Dispersion is $r > v$, moderate. The optical orientation is $X = \mathbf{a}$, $Y = \mathbf{c}$, $Z = \mathbf{b}$. The calculated density is $3.06 \text{ g}\cdot\text{cm}^{-3}$. Electron microprobe analyses together with crystal structure refinement results gives the empirical formula



$((As_{0.65} P_{0.35})O_4)_2 O_{5.86} (OH)_{1.14}$. Alcantarillaite is orthorhombic, with an average-structure described in *Imma*, and with $a = 24.038(8) \text{ \AA}$, $b = 7.444(3) \text{ \AA}$, $c = 10.387(3) \text{ \AA}$, $V = 1858.6(11) \text{ \AA}^3$ and $Z = 4$. The structure ($wR_{\text{obs}} = 0.078$ for 651 reflections to a resolution of 0.91 \AA) differs most significantly from other walentaite-group members in having an interlayer *A2* site occupied. Square-pyramidal polyhedra centred at the *A2* sites form edge-shared dimers, $(Fe^{3+})_2 O_4 (H_2O)_4$. The dimers share vertices with TO_4 anions in the layers on either side to form 8-sided channels along $[010]$ occupied by H_2O molecules.

Keywords: alcantarillaite, new mineral, walentaite group, crystal structure, Alcantarilla mine, walentaite, natrowalentaite, halilsarpite

Introduction

Walentaite (Dunn *et al.*, 1984; Grey *et al.*, 2019a), natrowalentaite (Nickel, 1987; Grey *et al.*, 2019b), halilsarpite (Husdal *et al.*, 2020) and alcantarillaite (this study) form an isostructural series of minerals with orthorhombic symmetry, space group *Imma*, $a \approx 24\text{--}26 \text{ \AA}$, $b \approx 7.4 \text{ \AA}$, $c \approx 10.4 \text{ \AA}$. Their general structural formula is

$[(A_1 A_1'_{1-y}), A_2](H_2O)_n [B_x (As_2)_{2-x} (As_3) M_1 (M_2)_2 (TO_4)_2 (O, OH)_7]$, based on heteropolyhedral layers $[M_1 (M_2)_2 (TO_4)_2 (O, OH)_6]$ with surface-coordinated species at the *B*, *As2* and *As3* sites, and with interlayer hydrated cation groups centred at the *A* sites. The minerals all have dominant As^{3+} at the *As* sites and Fe^{3+} at the *M* sites and are distinguished chemically by different predominant cations at the *A*, *B* and *T* sites, and on this basis, they form a mineral group as defined by Mills *et al.* (2009). A proposal for a walentaite group, with the group name based on the first mineral in the group to be characterized has been approved by the Commission on New Minerals, Nomenclature and Classification (CNMNC) of the International Mineralogical Association (IMA).

Alcantarillaite is the newest member of the group. The characterization of alcantarillaite is presented in the following sections. The name is for the locality. The new mineral and its name have been approved by the CNMNC (IMA2019-072). Portions of the Alcantarilla mine holotype sample used in the study are deposited in the Mineralogical State Collection Munich (collection number MSM37182) and at the Natural History Museum, Oslo (collection number KNR44147). Crystals from the holotype are deposited as a cotype in the collections of the Natural History Museum of Los Angeles County, 900 Exposition Boulevard, Los Angeles, CA 90007, USA, catalogue number 73568.

Occurrence

Alcantarillaite was identified on specimens from the Alcantarilla wolframite mine (Mina Nuestra Senora de Los Alcantarillas), Belalcazar, Cordoba, Andalusia, Spain (38°N, 5°W). The Alcantarilla mine is host to many secondary iron arsenites and arsenates including karibibite, toelite, pharmacosiderite and schneiderhöhnite (Rewitzer *et al.*, 2016). The specimens, including the type specimen, were obtained from within boulders at the mine dumps, but the mineral has also been found underground in a gallery by excavating löllingite pods in quartz. Alcantarillaite most commonly is observed as lemon-yellow fillings together with massive scorodite in fissures and cracks in quartz adjacent to löllingite. It is also found as tiny rosettes lining vugs and as spheroids of ultrathin blades. From investigations on numerous samples, the main associations observed were alcantarillaite sitting on scorodite, on toelite, on karibibite and on pharmacosiderite. Toelite, karibibite and pharmacosiderite were also often found on scorodite. Primary mineral sources for the cations in alcantarillaite are löllingite (As, Fe) and ferberite (W, Fe).

Physical properties

The alcantarillaite crystals used for the determination of physical properties were in the form of ultra-thin elongated blades, with lengths up to 0.1 mm and thicknesses of only 1-2 μm (Figures 1 and 2). The crystals are generally curved, and show sub-parallel lamellae. They are lemon-yellow in colour with a pale-yellow streak and vitreous lustre. The crystals are brittle with uneven fracture and perfect cleavage on $\{100\}$. The calculated density is $3.06 \text{ g}\cdot\text{cm}^{-3}$ based upon the empirical formula and single-crystal XRD cell.

Optically alcantarillaite crystals are biaxial (-), with $\alpha = 1.703(\text{calc})$, $\beta = 1.800(5)$, $\gamma = 1.850(5)$ (white light). The measured $2V$ is $68(1)^\circ$ from extinction data analysed using the program EXCALIBR (Gunter *et al.*, 2004). The dispersion is $r > v$, moderate, and the optical orientation is $X = \mathbf{a}$, $Y = \mathbf{c}$, $Z = \mathbf{b}$. No pleochroism was observed. Because α is perpendicular to the very thin plates, it could not be measured reliably; consequently, it has been calculated from β , γ and $2V$.

Raman spectroscopy

The Raman spectrum of alcantarillaite was obtained using a Horiba XploRA system, mounted on an Olympus BX51 microscope, at the Mineralogical State Collection, Munich. By using a $100\times$ long-distance objective, it was possible to obtain spectra from samples with a very small cross section ($\sim 20 \mu\text{m}$). The spectra were obtained in a spectral range of $50\text{--}4000 \text{ cm}^{-1}$ using a 532 nm laser. The background was subtracted by a polynomial fitting, implemented in the Horiba LabSpec Software (version 5). Peak analysis was performed by using the PeakFit Software (version 4.12). The location of bands in the region 50 to 1100 cm^{-1} was carried out using the Gaussian convolution method. The bands were fitted by a combination of Gaussian and Lorentzian peaks, successively optimized by iteration method, up to a squared correlation coefficient of r^2 greater than 0.990.

The Raman spectrum is shown in Figure 3(a) for the region 2500 to 4000 cm^{-1} (region of O-H stretching) and in Figure 3(b) for the region 0 to 1100 cm^{-1} . Figure 3(a) shows two weak, sharp hydroxyl stretching bands at 3506 and 3580 cm^{-1} superimposed on a very broad band, centred at $\sim 3100 \text{ cm}^{-1}$, due to hydrogen-bonded H_2O . The interpretation of the spectrum in the region 50 to 1100 cm^{-1} is complicated by the existence of both As^{3+} and As^{5+} together with W^{6+} , so there are many overlaps. Assignments are very tentative.

The bands at 801 and 813 cm^{-1} can be assigned to the AsO_4 -stretching mode. In comparison with the spectrum of leiteite ZnAs_2O_4 (Frost and Bahfenne, 2009) the band at 453 cm^{-1} can be assigned to the $\nu_2 \text{As}_2\text{O}_4^{2-}$ bending mode. A band at 419 cm^{-1} can be tentatively assigned to the δAsO_2 bending mode according to Bencivenni and Gingerich (1983). The band at 830 cm^{-1} could be tentatively assigned to the AsO_3^{2-} symmetric stretching mode (Frost & Bahfenne, 2009). W-O stretching bands mostly should be hidden under the dominating As-O stretching vibrations. In

comparison with the data in the paper of Frost *et al.* (2004) on Raman microscopy of selected tungstate minerals, the peaks at 891 and 948 cm^{-1} could be attributed to the W-O stretching vibrations as well as the peak at 782 cm^{-1} . Note that an energy-dispersive analysis of the specimen used for the Raman spectroscopy showed negligible phosphorus, in agreement with the lack of P-O stretching vibration bands in Figure 3(b).

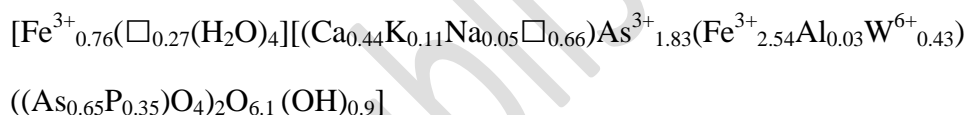
In the full scan, 50 to 4000 cm^{-1} , there was no H_2O bending mode peak evident in the region 1500 to 1700 cm^{-1} . From experience on related walentaite-group minerals, this is most likely due to the H_2O being driven off by laser-beam heating before the scan got to the bending-mode region.

Chemical composition

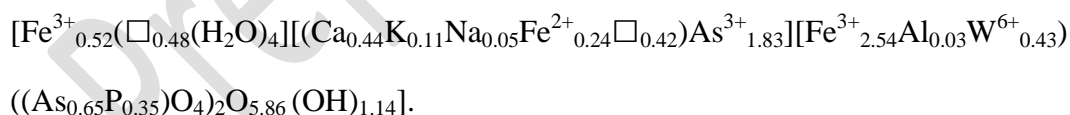
Alcantarillaite crystals were mounted in a polished section and analysed using wavelength-dispersive spectrometry on a JEOL JXA 8500F Hyperprobe operated at an accelerating voltage of 15 kV and a beam current of 4 nA. The beam was defocused to 1-2 μm . Analytical results (average of single analyses on 4 crystals) are given in Table 1. The $\text{As}_2\text{O}_3/\text{As}_2\text{O}_5$ were apportioned to give $2(\text{As}^{5+} + \text{P})$ tetrahedral *apfu*, in accordance with the crystal structure. The H_2O was calculated based on the crystal structure. The results are given in Table 1. The atomic fractions, based on $\text{O} = 19$ *apfu* in accord with the structure are:



Expressing the atomic fractions in structural form gives the formula:



This formula deviates somewhat from the refined site occupancies for the *A* and *B* sites, as discussed in the structure refinement section. If a small portion of the iron is assigned as Fe^{2+} and located with Ca at the *B* site, the following empirical formula is obtained:



The ideal formula is $[\text{Fe}^{3+}_{0.5}\square_{0.5}(\text{H}_2\text{O})_4][\text{CaAs}^{3+}_2(\text{Fe}^{3+}_{2.5}\text{W}^{6+}_{0.5})(\text{AsO}_4)_2\text{O}_7]$, which requires Fe_2O_3 26.30, CaO 6.16, WO_3 12.72, As_2O_3 21.71, As_2O_5 25.22, H_2O 7.90, Total 100 wt.%.

Crystallography

Powder X-ray diffraction

Several crystals of alcantarillaite mounted with oil on a cryo loop were used to collect powder XRD data with a Rigaku Synergy-S diffractometer, equipped with a hybrid photon counting area detector (HyPix6000HE). Data was collected in the two-theta range 4 to 82° using monochromatized $\text{CuK}\alpha$

radiation. A Gandolfi-like motion on the ϕ and ω axes was used to randomize the sample. The background was removed from the scan and Rietveld refinements were made using FULLPROF (Rodriguez-Carvajal, 1990). The atomic parameters were taken from the single crystal refinement and only profile parameters were refined, giving refined unit cell parameters $a = 24.025(16)$ Å, $b = 7.418(4)$ Å, $c = 10.348(7)$ Å and $V = 1844(3)$ Å³. The indexed powder XRD pattern for alcantarillaite is given in Table 2.

Single-crystal studies

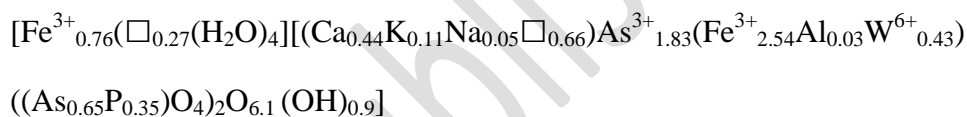
A thin blade of alcantarillaite, $0.100 \times 0.020 \times 0.002$ mm³ was mounted in a fibre loop for a data collection made at the macromolecular beam line MX2 of the Australian Synchrotron. The MX2 beamline utilises an Eiger 16M detector operating at 100 Hz. Data were collected using monochromatic radiation with a wavelength of 0.7107 Å. The sample was placed in a stream of nitrogen gas at 100K maintained using an Oxford Cryosystems ScryoStream 800 throughout the duration of the experiment. The experiment itself consisted of a single sweep of 360 degree rotation around phi. The crystal of alcantarillaite was exposed to x-rays for a total of 36 seconds (whilst the detector acquires the data), the resulting dataset consists of 3600 individual images with an approximate phi angle of each image being 0.1 degrees. Prior to undertaking a final collection, individual snapshots of 20 degrees (200 images) were undertaken to test the quality of the crystal and the required attenuation level. The best area of the sample to allow a full collection was located (towards the tip of the sample) and a level of attenuation of between 20% – 50% chosen during the collection. The resulting simulated diffraction pattern (merging of $10 \times 0.1^\circ$ frames) showed no signs of superstructure reflections, but showed weak diffuse reflections at higher angles. The raw intensity dataset was processed using XDS software to produce data files that were analysed using JANA2006 (Petříček *et al.*, 2014). Data collection and refinement conditions are given in Table 3.

Structure refinement

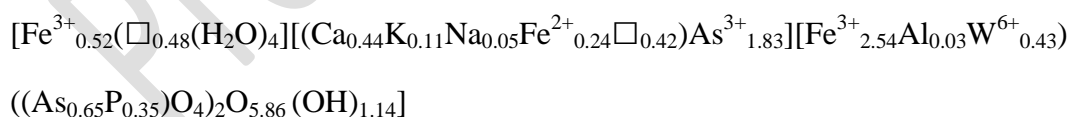
The atomic coordinates for natrowalentaite in space group *Imma* (Grey *et al.*, 2019b) were used to start the refinement, with As⁵⁺ in place of P⁵⁺ at the tetrahedral *T* site. The *M2* and *T* sites were refined with joint occupancies by W/Fe and As/P, respectively. Refinement of the partially occupied *A1* and *A1'* sites and *Ow* (H₂O) sites in the interlayer region resulted in their occupancy factors going to zero. Difference-Fourier maps showed a new configuration of interlayer species involving metal atoms, in site *A2*, coordinating to two apical oxygen atoms, *O1*, of *TO*₄ in adjacent layers as well as to three interlayer H₂O (*Ow1* and *Ow2*). The resulting *A2O*₂(H₂O)₃ square-pyramids form dimers by edge-sharing as shown in Figure 4. The mean *A2*-O bond distance of 1.98 Å and the bond-valence sum for Fe at *A2* of 2.94 valence units (Gagné and Hawthorne, 2015) are

consistent with Fe³⁺ occupying the A2 site. Several partially-occupied sites containing uncoordinated H₂O molecules were also located in difference-Fourier maps (Ow3 to Ow6). With anisotropic displacement parameters for the heteropolyhedral layer atoms and isotropic displacement parameters for the partially occupied interlayer species and surface-coordinated cations (see Table 4), the refinement converged to $wR_{\text{obs}} = 0.078$ for 651 observed reflections to a resolution of 0.91 Å. Although the data was collected to a resolution of 0.69 Å, the extremely small and curved nature of the crystal resulted in a marked deterioration of data quality at higher angles. An upper resolution limit of 0.91 Å was chosen based on where the merging *R* factor for equivalent reflections showed a steep increase. Other details of the refinement are given in Table 3. Sigma weights were used. The high *GofF* is not unusual for refinements using JANA, where the weighting scheme is not adjusted to minimize the *GofF*. The refined atom coordinates and equivalent isotropic displacement parameters are reported in Table 4, anisotropic displacement parameters in Table 5 and polyhedron bond distances are given in Table 6. The displacement parameters reported in Table 4 are quite high, particularly for the water molecule sites. This is a consequence of the very weak diffraction data obtained on the ultra-thin crystal, and problems in attempting to refine both displacement parameters and site occupancies for partially occupied sites.

The refined site occupancies for the A2 and B sites in Table 4 showed a discrepancy when compared with assignments based on the EMP analyses. The empirical formula, expressed in structure form and based on the EMP analyses is:



The site occupancy refinements (Table 4) gave only 0.52 Fe at the A2 site and 0.68 atoms (using Ca electron-scattering in the refinement) at the B site. A possible explanation for this discrepancy is that a small fraction of the Fe is present as Fe²⁺, and it is located at the B site. Transferring 0.24 Fe as Fe²⁺ from the A2 site to the B site gives the empirical formula



The occurrences of alcantarillaite are so sparse that it was not possible to quantify the Fe²⁺ content, for example by Mossbauer spectroscopy. We obtained a positive qualitative test for ferrous iron by adding potassium ferricyanide to an acid solution of dissolved alcantarillaite crystals and observing an intense blue coloration due to the formation of a mixed ferri-ferrocyanide complex. It is worth noting that schneiderhöhnite, a mineral associated with alcantarillaite, is a mixed valence iron arsenite, Fe²⁺Fe³⁺₃As³⁺₅O₁₃.

Discussion

An [010] projection of the average crystal structure of alcantarillaite in space group *Imma* is given in Figure 4. This figure shows the $[M1(M2)_2(TO_4)_2(O,OH)_6]$ heteropolyhedral layers with surface-coordinated *B*-site cations and with interlayer edge-shared dimers of 5-coordinated *A2*-site cations and H₂O molecules. A view along approximately [100] of the interlayer polyhedra (Figure 5) shows that the 5-coordinated *A2*-site cations form zig-zag edge-shared chains along [010]. The *A2*-*A2* separations along the chains are alternately 3.07 and 1.64 Å. The latter separation is much too short for both sites to be simultaneously occupied, and so only one of the pairs of *A2* sites can be occupied locally. This then gives dimers of edge-shared square-pyramids, with *A2*-*A2* = 3.07 Å. The dimers are locally oriented either close to [011] or to [0-11] and which dimer is occupied will likely be related to the occupancies of the *M2* and *As2* sites in the adjacent layers. The 5-coordinated square-pyramids centred at site *A2* represent a major departure from interlayer species in other walentaite-group minerals. Walentaite, natrowalentaite and halilsarpite all contain $A1(H_2O)_6$ octahedra and $A1'(H_2O)_4(H_2O)_{4/2}$ square-antiprisms, which hold the heteropolyhedral layers together by hydrogen-bonding. In contrast, the $(A2)_2O_4(H_2O)_4$ dimers in alcantarillaite directly bond to the heteropolyhedral layers by sharing vertices with TO_4 tetrahedra. This direct bonding entails a considerable reduction in the interlayer spacing (= $0.5a$) from about 13 Å in walentaite, natrowalentaite and halilsarpite to only 12 Å in alcantarillaite. The reduction in interlayer spacing is associated with a decrease in the number of interlayer H₂O molecules from 6 to 4 *pfu*. As seen in Figure 4, the structure of alcantarillaite contains eight-sided channels along [010] occupied by H₂O molecules and is more correctly described as a 3D framework structure rather than a layer structure.

Alcantarillaite, in common with natrowalentaite, has minor substitution of W^{6+} for Fe^{3+} at the *M2* site. The W^{6+} is displaced by 0.47 Å from the $8i$ position occupied by Fe^{3+} to the general position $16j$, labelled *M2'* in Table 4. In this position the W^{6+} has two short W-O bonds, 1.65 Å (Table 6) characteristic of the tungstenyl group (Roy *et al.*, 2015). The partial substitution of M^{6+} for Fe^{3+} at *M2* is counterbalanced by a decrease in the As^{3+} content. As shown by the ideal formulae given in the next section, walentaite has no M^{6+} at *M2*, and has 3 As^{3+} per formula unit, whereas natrowalentaite, halilsarpite and alcantarillaite, all with M^{6+} substitution at *M2*, have only 2 As^{3+} per formula unit (and corresponding increases in the *B*-site occupancy).

The *As2* and *As3* surface-coordinated sites, occupied by As^{3+} , are shown in Figure 6(a) for the average structure. Both sites are split from special positions. The *As2* site is split into doublets, separated by 0.23 Å from the $8f$ position ($x,0,0$) and the *As2* site is split into quadruplets, separated by 0.92 Å from the $4d$ position, $(\frac{1}{4},\frac{1}{4},\frac{3}{4})$. We have previously reported (Grey *et al.*, 2019a,b, Husdal *et al.*, 2020) that a possible locally ordered configuration is a trimeric cluster, $As3(As2)_2O_6$, in which pairs of corner-connected $(As2)O_3$ trigonal pyramids share an edge with $(As3)O_3$. A

reviewer has pointed out, however, that the *As2-As3* shared-edge separation in alcantarillaite is unreasonably short, 2.65 Å. In addition, the cluster involves all three As^{3+} cations sharing a common anion, O6, with a formal valency of 3, and it would be expected to be unstable. We have further examined different locally ordered occupancies of the different *As2* and *As3* sites and have identified an alternative configuration, in space group *Imm2*, that is a linear trimer of corner-shared trigonal pyramids with formula $\text{As}_3(\text{As}_2)_2\text{O}_7$, shown in Figure 6(b). The *As2-As2* and *As2-As3* distances are 3.33 and 3.06 Å, respectively. A similar $[\text{As}^{3+}_3\text{O}_7]^{5-}$ linear trimer has been reported for the heteropolymolybdate, $[\text{As}^{3+}_3\text{Mo}_3\text{O}_{15}]^{3-}$ by Martin-Frère *et al.* (1999). The As_3O_7 cluster has an extra anion relative to the As_3O_6 cluster and its presence should be verifiable from refined anion site occupancies in the average *Imma* structure. Refinements of the *As2*, *As3* and O6 site occupancies in walentaite-group minerals (Grey *et al.*, 2019a,b, Husdal *et al.*, 2020), however, are more consistent with a As_3O_6 cluster composition than a As_3O_7 cluster. Single-crystal XRD refinements of better-diffracting crystals and/or neutron diffraction refinements are needed to confirm the configurations of locally ordered $\text{As}^{3+}_n\text{O}_m$ clusters.

The distribution of surface-coordinated sites is further complicated by the *As2* and *B* sites being separated by only 0.9 Å, so that their occupations are mutually exclusive, giving the configuration $(B_x(\text{As}_2)_{2-x})$ in the general formula. The crystal structure comprises numerous possible local configurations of surface-coordinated cations and the *Imma* structure represents an average of all such local configurations. One consequence of this, verified from single-crystal refinements of the four walentaite group members, is that the As^{3+} -O distances are longer than normally observed for arsenite minerals, as discussed by Grey *et al.* (2019a).

The interlayer cation sites are also split, with *A1* and *A1'* separated by only ~1.2 Å in walentaite, natrowalentaite and halilsarpite, and the *A2* site in alcantarillaite is split into doublets separated by 0.82 Å from the *4e* position $(0, \frac{1}{4}, z)$. There is evidence, from the study on walentaite (Grey *et al.*, 2019a) that the occupation of the surface-coordinated cation sites and the interlayer sites are correlated, so that locally there are regions (microdomains) of one or the other of the following two configurations:

1. $[\text{A1}(\text{H}_2\text{O})_6][(\text{As}_2)_2(\text{As}_3)\text{M1}(\text{M}_2)_2(\text{TO}_4)_2(\text{O},\text{OH})_7]$
2. $[\text{A1}'(\text{H}_2\text{O})_6][(\text{B}_2)_2(\text{As}_3)\text{M1}(\text{M}_2)_2(\text{TO}_4)_2(\text{O},\text{OH})_7]$

In walentaite, the site occupancies are consistent with 80% of configuration 1 and 20% of configuration 2. In the other three minerals there are approximately equal proportions of the two configurations, giving $(B_{0.5}(\text{As}_2)_{0.5})_2$ for the close-positioned sites *B/As2*.

The walentaite group

The general structural formula for walentaite-group minerals is:

$[(A1_y A1'_{1-y}), A2](H_2O)_n [B_x (As2)_{2-x} (As3) M1 (M2)_2 (TO_4)_2 (O, OH)_7]$, where $n = 4$ for alcantarillaite

and $n = 6$ for the other three minerals. The cation substitutions at the different sites for the

walentaite-group minerals are given in Table 7, with the dominant cation listed first. Walentaite and natrowalentaite each have P^{5+} dominant at the T site whereas halilsarpite and alcantarillaite have dominant As^{5+} at the T site. On this basis the walentaite group is subdivided into walentaite and halilsarpite subgroups based on the dominant cation at the T site being P^{5+} or As^{5+} , respectively.

A general chemical formula for the four minerals is $[A(H_2O)_n][B_x C_{3-x}]M_3(TO_4)_2(O, OH)_7$, where A, C and M include the atoms at $A1+A1'+A2$, $As2+As3$ and $M1+M2$ sites respectively. The ideal formulae for the minerals are:

walentaite: $[Mn(H_2O)_6][\square As^{3+}_3 Fe^{3+}_3 (PO_4)_2 O_7]$

natrowalentaite: $[Fe_{0.5} Na_{0.5} (H_2O)_6][Na As^{3+}_2 (Fe^{3+}_{2.33} W^{6+}_{0.67}) (PO_4)_2 O_7]$

halilsarpite: $[Mg(H_2O)_6][Ca As^{3+}_2 (Fe^{3+}_{2.67} Mo^{6+}_{0.33}) (AsO_4)_2 O_7]$

alcantarillaite: $[Fe^{3+}_{0.5} \square_{0.5} (H_2O)_4][Ca As^{3+}_2 (Fe^{3+}_{2.5} W^{6+}_{0.5}) (AsO_4)_2 O_7]$

Only for walentaite does the ideal formula correspond to an end-member formula as recommended by the IMA-CNMNC guidelines (Bosi *et al.*, 2019). As discussed in the previous section, walentaite has a dominant (80%) configuration 1 component and the end-member formula is based on this component. For the other three minerals there are approximately equal contributions of the two configurations and giving one or the other as an end-member formula would provide information incompatible with the crystal structure. They correspond to mid-member compositions.

Further elucidation of the local-ordered structures of these minerals requires refinements for crystals with higher diffracting quality to get greater precision for the parameters of the atoms in partially occupied, split sites. Finding more abundant occurrences of the sparsely distributed minerals would help by having large-enough quantities for neutron diffraction to better-characterise the anions. Pair-distribution function analysis would also be helpful in distinguishing between different local configurations.

Acknowledgments

We thank Fernando Camara, Peter Leverett and an anonymous reviewer for their very helpful comments. This research was undertaken in part using the MX2 beamline at the Australian Synchrotron, part of ANSTO, and made use of the Australian Cancer Research Foundation (ACRF) detector.

Prepublished Article

References

- Bencivenni, L. and Gingerich, K.A. (1983) The characterization of alkali arsenites and antimonites: the IR spectra of matrix-isolated MAsO_2 and MSbO_2 molecules. *Journal of Molecular Structure*, **99**, 23–29.
- Bosi, F., Hatert, F., Halenius, U., Pasero, M., Miyawaki, R. and Mills, S.J. (2019) On the application of the IMA-CNMNC dominant-valency rule to complex mineral compositions. *Mineralogical Magazine*, **83**, 627–632.
- Dunn, P.J., Peacor, D.R., Roberts, W.L., Campbell, T.J. and Ramik, R.A. (1984) Walentaite, a new calcium iron arsenate phosphate from the White Elephant Mine, Pringle, South Dakota. *Neues Jahrbuch für Mineralogie, Monatshefte*, **1984**, 169–174.
- Frost, R.L. and Bahfenne, S. (2010) Raman spectroscopic study of the arsenite minerals leitite ZnAs_2O_8 , reinerite $\text{Zn}_3(\text{AsO}_3)_2$ and cafarsite $\text{Ca}_5(\text{Ti,Fe,Mn})_7(\text{AsO}_3)_{12}\cdot 4\text{H}_2\text{O}$. *Journal of Raman Spectroscopy*, **41**, 325–328.
- Frost, R.L., Duong, L., and Weier, M. (2004) Raman microscopy of selected tungstate minerals. *Spectrochimica Acta, Part A, Molecular and biomolecular spectroscopy*, **60**, 1853–1859.
- Gagné, O.C. and Hawthorne, F.C. (2015) Comprehensive derivation of bond-valence parameters for ion pairs involving oxygen. *Acta Crystallographica*, **B71**, 562–578.
- Grey, I.E., Mumme, W.G. and Hochleitner, R. (2019a) Trimeric $\text{As}^{3+}_3\text{O}_6$ clusters in walentaite: Crystal structure and revised formula. *European Journal of Mineralogy*, **31**, 111–116.
- Grey, I.E., Mumme, W.G., Kampf, A.R., MacRae, C.M. and Wilson, N.C. (2019b) Natrowalentaite, a new mineral from the Griffins Find gold deposit, Western Australia. *Australian Journal of Mineralogy*, **20**, 7–15.
- Husdal, T., Grey, I.E., Friis, H., DaL Bo, F., Kampf, A.R., MacRae, C.M., Mumme, W.G., Ljøstad, O.-T. and Shanks, F. (2020) Halilsarpite, a new arsenate analogue of walentaite, from the Oumlil mine, Bou Azzer district, Morocco. *European Journal of Mineralogy*, **32**, 89–98.
- Gunter, M.E., Bandli, B.R., Bloss, F.D., Evans, S.H., Su, S.C., and Weaver, R. (2004) Results from a McCrone spindle stage short course, a new version of EXCALIBUR, and how to build a spindle stage. *The Microscope*, **52**, 23–39.
- Martin-Frère J., Jeannin Y., Robert F. and Vaisserman J. (1991) Synthesis and X-ray structures of two unprecedented heteropolymetalates $[\text{As}_3\text{M}_3\text{O}_{15}]^{3-}$ ($\text{M} = \text{Mo}, \text{W}$) and $[\text{As}_6\text{CoMo}_6\text{O}_{30}]^{4-}$. First examples of linear triarsenate(III) and cyclic triarsenate(III). *Inorganic Chemistry*, **30**, 3635–363
- Mills, S.J., Hatert, F., Nickel, E.H. and Ferraris, G. (2009) The standardisation of mineral group hierarchies: application to recent nomenclature proposals. *European Journal of Mineralogy*, **21**, 1073–1080.
- Nickel, E.H. (1987) Tungsten-bearing walentaite from Griffins Find gold deposit, Western Australia. *Australian Mineralogist*, July 1987, 9–12.
- Petříček, V., Dušek, M., and Palatinus, L. (2014) Crystallographic Computing System JANA2006: General features. *Zeitschrift für Kristallographie*, **229**, 345–352.
- Rewitzer C., Hochleitner R., Fehr T., and Utrera C. (2016) Karibibite, schneiderhöhnite, tooeleite and other uncommon secondary minerals in the Nuestra Señora de las Alcantarillas mine, Belalcázar, Córdoba, Spain; MineralUp (Revista de Minerales) No.1 Oct. 2016, 9–39.

Rodriguez-Carvajal, J. (1990) FULLPROF: A Program for Rietveld Refinement and Pattern Matching Analysis. Satellite meeting on powder diffraction of the XV Congress of the IUCr, Toulouse, France, 1990.

Roy S.C., Raguz B., Assenmacher W. and Glaum R. (2015) Synthesis and crystal structure of mixed metal(III) tungstenyl(VI) orthopyrophosphates: *Solid State Sciences*, **49**, 18–28.

Prepublished Article



Figure 1. Spheroids of alcantarillaite blades. FOV 2.6 mm.

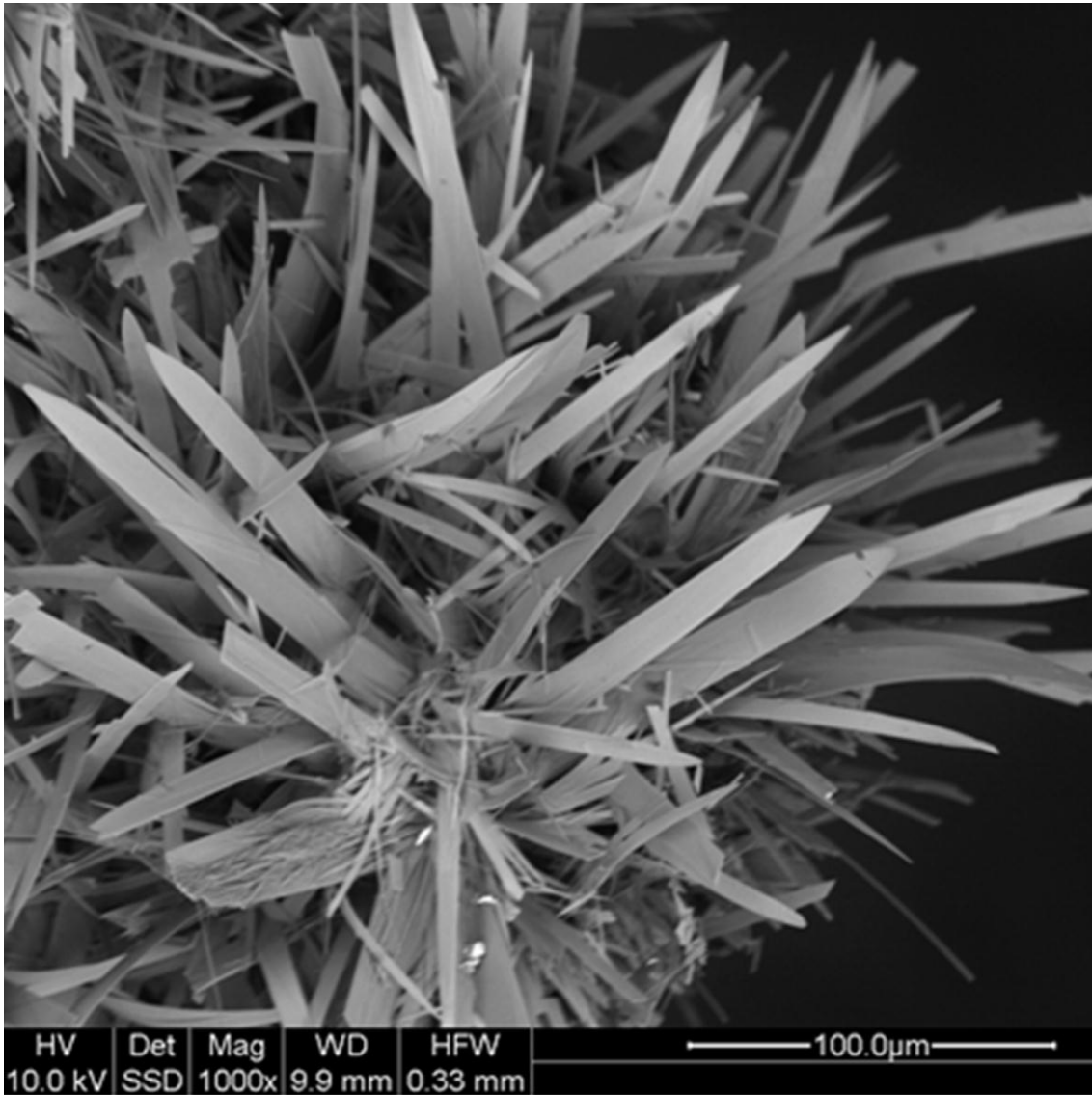


Figure 2. Back-scattered electron image of a cluster of blades of alcantarillaite.

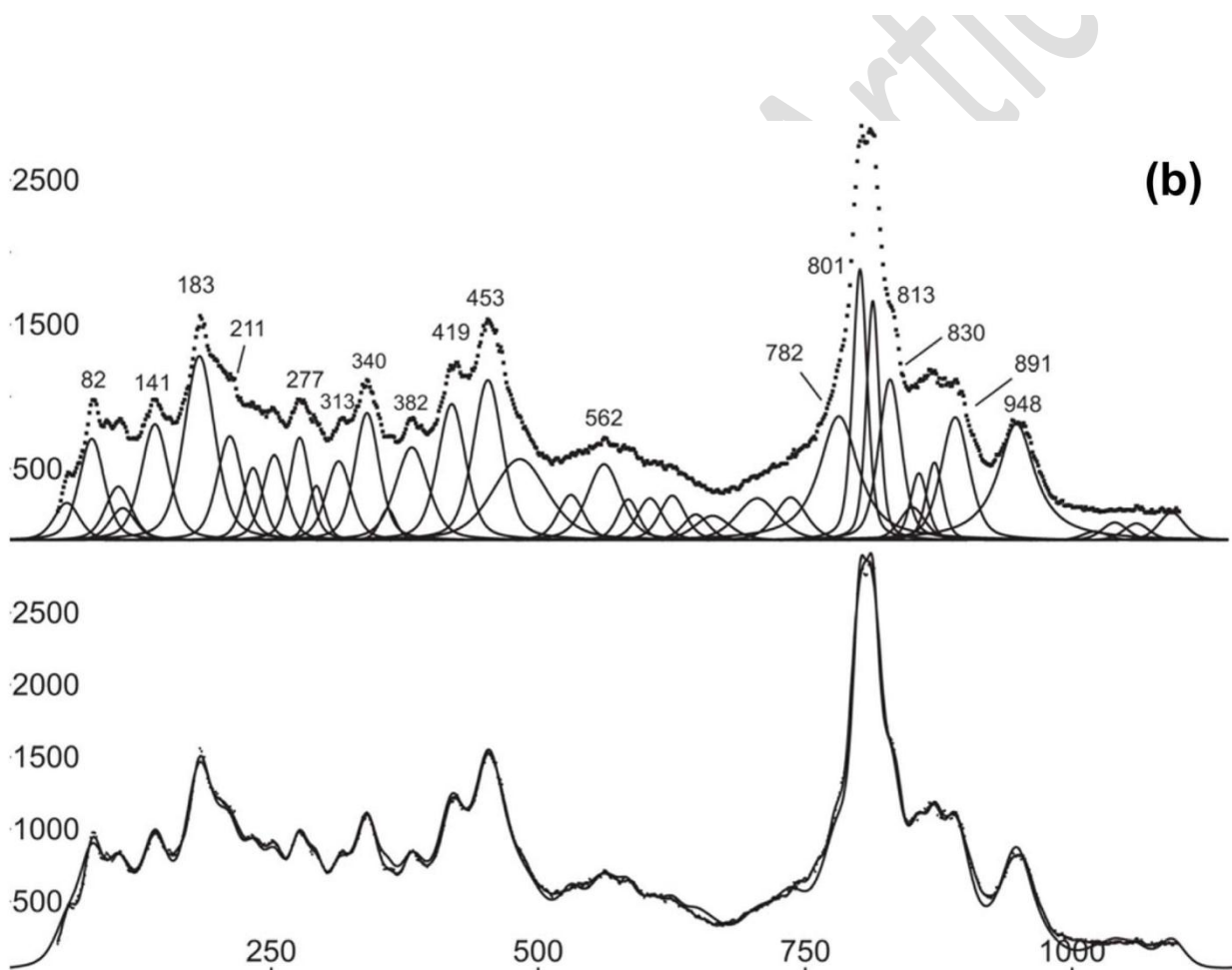
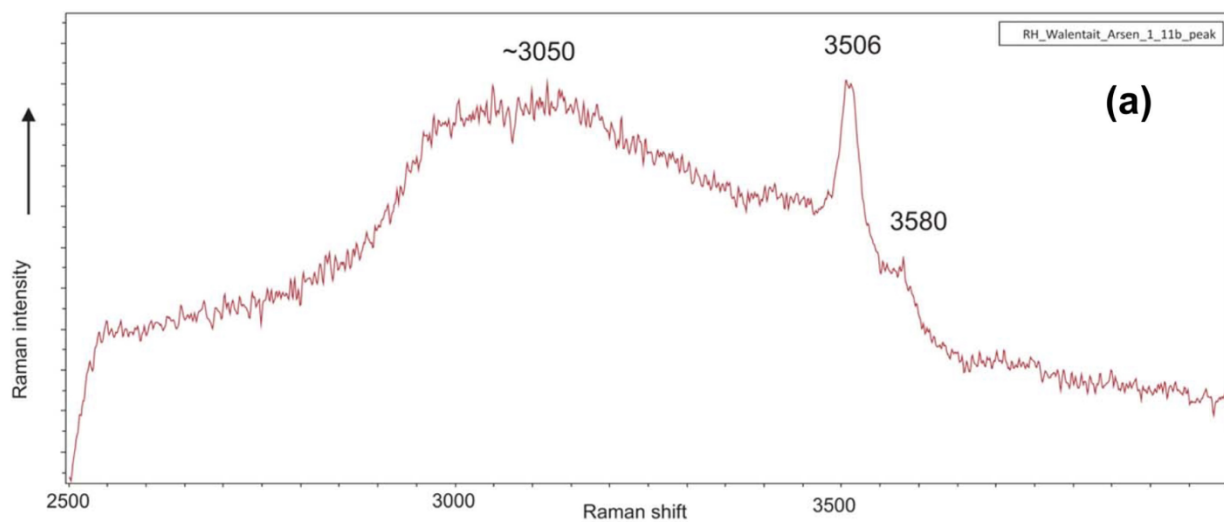


Figure 3. Raman spectra for alcantarillaite. (a) O-H stretching region, 2500 to 4000 cm^{-1} .

(b) Fitted spectrum in the range 50 to 1100 cm^{-1} .

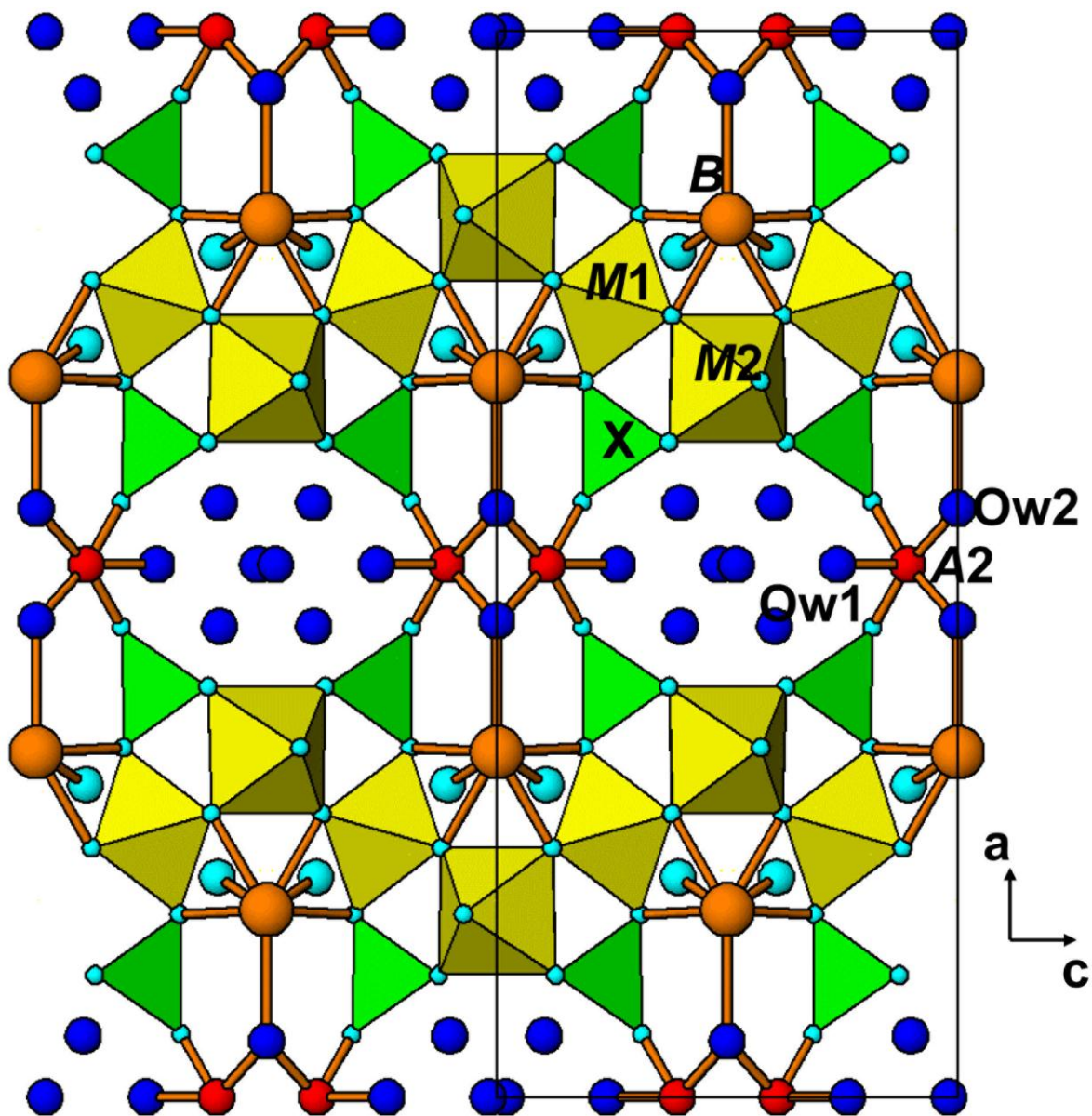


Figure 4. [010] projection of the alcantarillaite structure. Dark blue circles are H₂O.

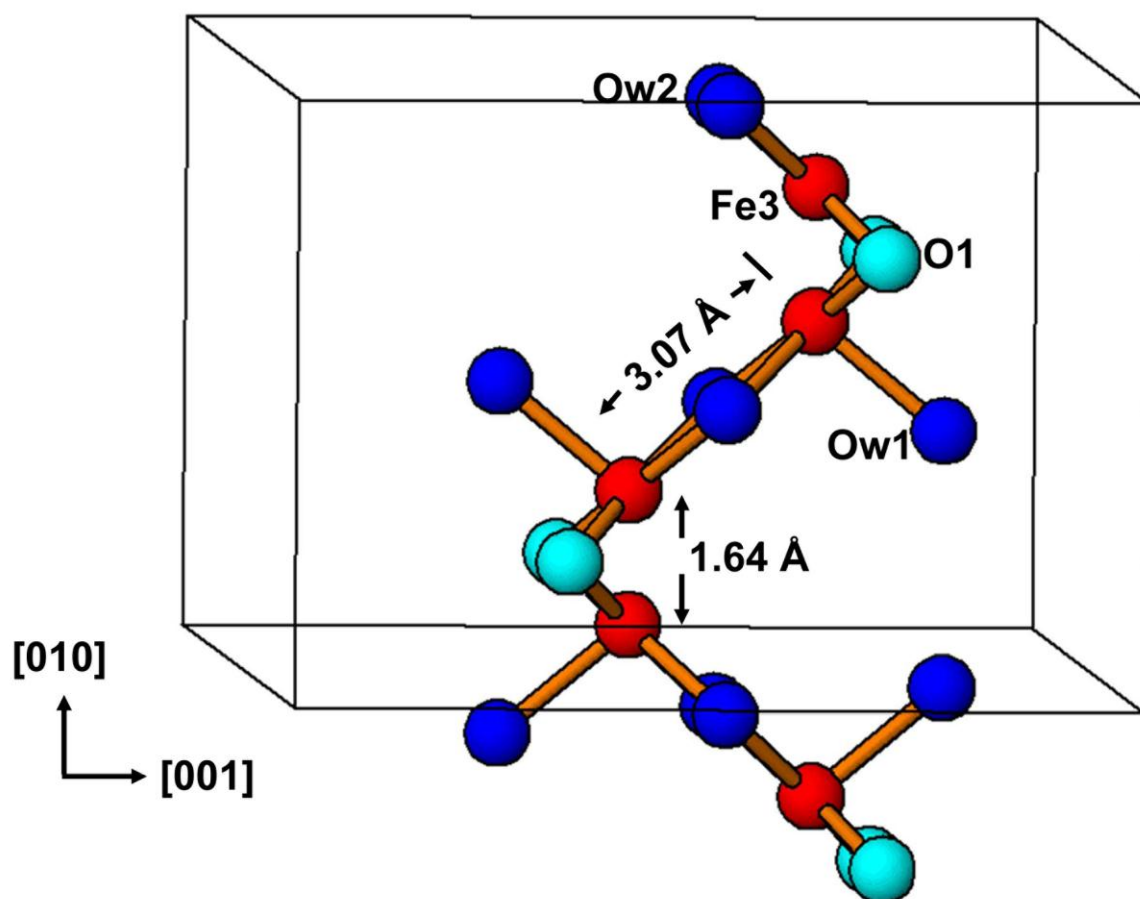


Figure 5. View approximately along [100] of interlayer 5-coordinated A2 sites..

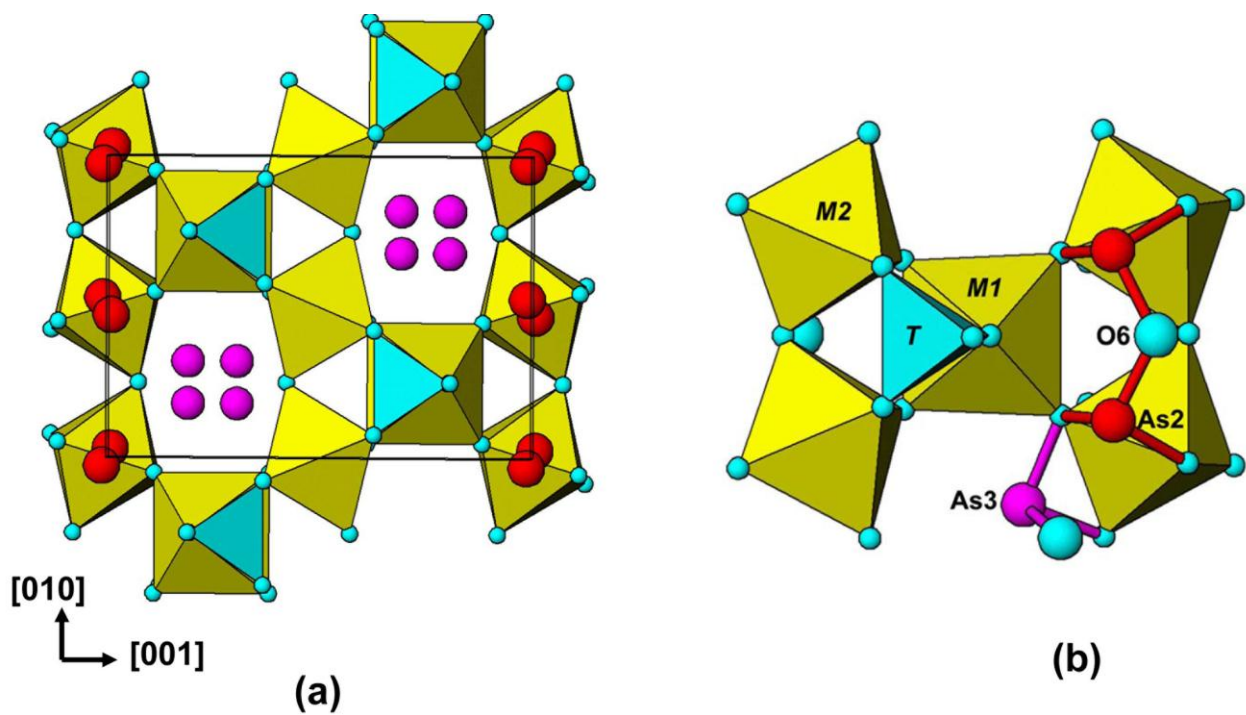


Figure 6. [100] projection of the structure of walentaite-group minerals showing (a) split As2 and As3 surface-coordinated cation sites and (b) a local ordering of As³⁺ in the As2 and As3 sites giving a [As³⁺₃O₇]⁵⁻ cluster.

Prepublished

Table 1. Analytical data (wt%) for alcantarillaite

	Mean	Range	SD	Reference Material
Na ₂ O	0.17	0.01-0.27	0.12	albite
K ₂ O	0.62	0.54-0.70	0.07	adularia
CaO	2.87	2.70-3.01	0.14	wollastonite
Al ₂ O ₃	0.20	0.08-0.28	0.07	MgAl ₂ O ₄
Fe ₂ O ₃	30.7	30.3-31.1	0.4	hematite
WO ₃	11.7	11.1-12.7	0.8	scheelite
P ₂ O ₅	5.85	5.36-6.65	0.56	berlinite
Total As as As ₂ O ₅	42.0	40.7-44.3	1.6	scorodite
As ₂ O ₃	21.1			
As ₂ O ₅	17.5			
H ₂ O	9.3			
Total	100.0			

Table 2. Powder X-ray data for alcantarillaite (d in Å).

I_{obs}	d_{meas}	d_{calc}	h	k	l
100	12.02	12.01	2	0	0
7	9.563	9.503	1	0	1
23	6.343	6.333	3	0	1
27	6.025	6.029	0	1	1
7	4.754	4.752	2	0	2
17	4.257	4.255	4	1	1
4	3.336	3.335	6	1	1
2	3.180	3.181	5	1	2
12	3.148	3.166	6	0	2
		3.128	0	1	3
38	3.016	3.015	0	2	2
11	2.927	2.924	2	2	2
6	2.592	2.597	8	0	2
		2.587	0	0	4
1	2.527	2.529	2	0	4
1	2.333	2.334	8	2	0
1	2.176	2.177	5	1	4
2	2.012	2.010	0	3	3
1	1.877	1.875	6	2	4
2	1.854	1.854	0	4	0
1	1.834	1.833	2	4	0
2	1.733	1.733	8	2	4
1	1.564	1.564	0	2	6
1	1.511	1.509	8	4	2
1	1.496	1.496	9	2	5

Table 3. Data collection and refinement conditions for alcantarillaite.

Atomic fractions	$\text{Na}_{0.05}\text{K}_{0.11}\text{Ca}_{0.44}\text{Al}_{0.03}\text{Fe}^{3+}_{3.30}\text{W}_{0.43}\text{As}^{3+}_{1.83}\text{As}^{5+}_{1.30}\text{P}_{0.70}\text{O}_{19}\text{H}_{8.9}$
Formula mass	855.6
Temperature	100 K
Wavelength	0.7107 Å
Crystal system, space group	Orthorhombic, <i>Imma</i>
Unit-cell dimensions	$a = 24.038(8)$ Å $b = 7.444(3)$ Å $c = 10.387(3)$ Å
Volume	$1858.6(11)$ Å ³
Z, Calculated density	4, 3.06 g cm ⁻³
Absorption coefficient	11.01 mm ⁻¹
Absorption correction	Empirical (SADABS). $T_{min} = 0.40$, $T_{max} = 0.75$
Crystal size	0.010 x 0.020 x 0.002 mm
Data resolution for refinement	0.91 Å
Reflections collected / unique / observed	15140 / 651 [$R_{int} = 0.101$] / 528
Range of indices	$-33 \leq h \leq 30$, $-9 \leq k \leq 9$, $-13 \leq l \leq 13$
Completeness to $\theta = 29.2^\circ$	98%
Refinement method	Full-matrix least-squares on F
Data / constraints / parameters	651 / 5 / 89
Final R indices [$I > 2\sigma(I)$]	$R_{obs} = 0.075$, $wR_{obs} = 0.077$
R indices (all data)	$R_{obs} = 0.088$, $wR_{obs} = 0.078$
$GofF$	3.54
Largest diff. peak and hole	1.27 and -1.32 e.Å ⁻³

Table 4. Refined coordinates, equivalent isotropic displacement parameters and site occupation factors (*sof*) for alcantarillaite.

Site	Wyckoff	<i>sof</i> *	X	y	z	U_{eq} (Å ²)
[M1(M2)₂(TO₄)₂O₆] layer						
M1	4c	0.25 Fe ³⁺	0.25	0.25	0.25	0.0593(15)
M2	8f	0.388(4) Fe ³⁺	0.3339(7)	0.5	0.5	0.060(4)
M2'	16j	0.112(4) W ⁶⁺	0.3155(8)	0.519(3)	0.495(2)	0.060(4)
T	8i	0.38(1) As ⁵⁺ 0.12(1) P	0.38593(11)	0.25	0.2800(2)	0.0626(10)
O1	8i	0.5	0.4419(6)	0.25	0.1872(16)	0.095(6)
O2	8i	0.5	0.3279(6)	0.25	0.1939(12)	0.070(5)
O3	16j	1	0.3856(4)	0.4315(11)	0.3727(7)	0.073(4)
O4a	16j	0.5	0.2762(8)	0.559(2)	0.6217(17)	0.052(3)
O4b	16j	0.5	0.2556(7)	0.562(3)	0.6186(19)	0.052(3)
O5	8i	0.5	0.3274(5)	0.25	0.5719(11)	0.063(4)
Surface-coordinated atoms						
As2	16j	0.264(7) As ³⁺	0.2123(3)	0.0261(9)	0.5131(7)	0.059(3)
As3	16j	0.216(7) As ³⁺	0.2716(3)	0.3076(7)	0.6920(6)	0.067(4)
B	8f	0.17(1) Ca	0.1759(9)	0	0.5	0.084(8)
O6	8i	0.29(1)	0.2056(8)	0.25	0.6063(18)	0.061081
Interlayer species						
A2	8h	0.129(5) Fe ³⁺	0.5	0.3608(14)	0.1082(9)	0.063(4)
Ow1	8h	0.129(5)	0.5	0.554(6)	0.261(4)	0.063(4)
Ow2	8f	0.26(1)	0.5581(9)	0.5	0	0.063(4)
Ow3	8i	0.18(2)	0.086(3)	0.25	0.697(7)	0.139(18)
Ow4	8i	0.18(2)	0.059(2)	0.25	0.891(5)	0.139(18)
Ow5	8h	0.08(2)	0	0.088(19)	0.014(13)	0.139(18)
Ow6	8i	0.22(2)	0.0605	0.25	0.7599	0.139(18)

**sof* multiplied by 4 gives the number of atoms per formula unit

Table 5. Anisotropic displacement parameters for alcantarillaite.

Atom	U^{11}	U^{22}	U^{33}	U^{23}	U^{13}	U^{12}
<i>M1</i>	0.089(3)	0.036(2)	0.053(2)	0	0.0041(18)	0
<i>M2</i>	0.088(10)	0.035(3)	0.057(2)	0	0	-0.0017(19)
<i>M2'</i>	0.088(10)	0.035(3)	0.057(2)	0	0	-0.0017(19)
<i>T</i>	0.091(2)	0.0413(14)	0.0550(14)	0	0.0026(12)	0
<i>O1</i>	0.092(12)	0.091(10)	0.101(11)	0	0.030(8)	0
<i>O2</i>	0.077(10)	0.066(8)	0.067(8)	0	0.001(7)	0
<i>O3</i>	0.121(8)	0.043(4)	0.055(5)	-0.004(5)	0.002(5)	-0.002(4)
<i>O5</i>	0.062(8)	0.044(6)	0.082(8)	0	0.004(6)	0

Table 6. Polyhedral distances in alcantarillaite (Å).

<i>M1</i> – <i>O2</i> x2 – <i>O4A</i> x4* – <i>O4B</i> x4*	1.961(14) 2.048(18) 1.960(19)	<i>T</i> – <i>O1</i> – <i>O2</i> – <i>O3</i> x2	1.654(16) 1.657(14) 1.659(8)
<i>M2</i> – <i>O3</i> x2 – <i>O4A</i> x2* – <i>O4B</i> x2* – <i>O5</i> x2	1.886(15) 1.93(2) 2.30(2) 2.011(5)	<i>M2'</i> – <i>O3</i> x2 – <i>O4A</i> x2* – <i>O4B</i> x2* – <i>O5</i> x2	2.21(2) 1.65(3) 1.96(3) 2.19(2), 1.87(2)
<i>As2</i> – <i>O4B</i> – <i>O4B</i> – <i>O6</i>	1.74(2) 1.648(19) 1.934(12)	<i>As3</i> – <i>O4A</i> – <i>O5</i> – <i>O6</i>	2.011(19) 1.881(13) 1.87(2)
<i>A2</i> – <i>O1</i> x2 – <i>Ow1</i> – <i>Ow2</i> x2	1.819(15) 2.14(4) 2.070(17)	<i>B</i> – <i>O2</i> x2 – <i>O4A</i> x2* – <i>O4B</i> x2* – <i>O6</i> x2 – <i>Ow2</i>	2.744(9) 2.76(3) 2.32(3) 2.278(13) 2.83(3)

*Split atoms 4A and 4B cannot be both present in same polyhedron.

Table 7. Minerals of the walentaite group, site constituents.

Mineral	A1	A1'	A2	B	As1	As2	M1	M2	T
<i>Walentaite subgroup</i>									
Walentaite	Mn ²⁺ , Fe ²⁺	Ca, Na	-	Ca, Na	As ³⁺	As ³⁺	Fe ³⁺	Fe ³⁺	P ⁵⁺ , As ⁵⁺
natrowalentaite	Fe ³⁺ , □	Na, Ca, □	-	Na, Ca, K, □	As ³⁺	As ³⁺	Fe ³⁺	Fe ³⁺ , W ⁶⁺	P ⁵⁺
<i>Halilsarpite subgroup</i>									
Halilsarpite	Mg, Fe ³⁺ , □	Mg, Ca, □	-	Ca, Mg, Na, □	As ³⁺	As ³⁺	Fe ³⁺	Fe ³⁺ , Mo ⁶⁺	As ⁵⁺
Alcantarillaite	-	-	Fe ³⁺ , □	Ca, K, Fe ²⁺ (?), □	As ³⁺	As ³⁺	Fe ³⁺	Fe ³⁺ , W ⁶⁺	As ⁵⁺ , P ⁵⁺